Circuit models for the co-simulation of superconducting quantum computing systems

Rohith Acharya*†, Fahd A. Mohiyaddin†, Anton Potočnik†, Kristiaan De Greve†, Bogdan Govoreanu†, Iuliana P. Radu†, Georges Gielen*†, Francky Catthoor†*

* Department of Electrical Engineering (ESAT), KU Leuven, Kasteelpark Arenberg 10, Leuven, B-3001, Belgium
† Imec, Kapeldreef 75, Leuven, B-3001, Belgium

***Abstract*—Quantum computers based on superconducting qubits have emerged as a leading candidate for a scalable quantum processor architecture. The core of a quantum processor consists of quantum devices that are manipulated using classical electronic circuits, which need to be co-designed for optimal performance and operation. As the principles governing the behavior of the classical circuits and the quantum devices are different, this presents a unique challenge in terms of the simulation, design and optimization of the joint system. A methodology is presented to transform the behavior of small-scale quantum processors to equivalent circuit models that are usable with classical circuits in a generic electrical simulator, enabling the detailed analysis of the impact of many important non-idealities. The methodology has specifically been employed to derive a circuit model of a superconducting qubit interacting with the quantized electromagnetic field of a superconducting resonator. Based on this technique, a comprehensive analysis of the qubit operation is performed, including the coherent control and readout of the qubit using electrical signals. Furthermore, the effect of several non-idealities in the system such as qubit relaxation, decoherence and leakage out of the computational subspace are captured, in contrast to previous works. As the presented method enables the co-simulation of the control electronics with the quantum system, it facilitates the design and optimization of near-term superconducting quantum processors.**

***Keywords*—Quantum computing, control electronics, co-simulation, equivalent circuit models, qubit readout, qubit control, non-idealities in quantum systems**

I. Introduction

Quantum computers based on superconducting qubits have made significant progress in the past two decades, and are well-positioned for the demonstration of prototype algorithms in the Noisy Intermediate Scale Quantum (NISQ) technology era with over 50 qubits [1]. A quantum advantage, dubbed as ‘quantum supremacy’, has also been demonstrated, where a quantum computer outperformed a classical supercomputer in performing a specific computational task [2]. To perform operations on a quantum processor, it is necessary to interface it with classical electronic control hardware, as shown in Fig. 1. With the scaling up of the number of qubits, the complexity of the electronic interface also increases, with several components operating at cryogenic temperatures [3], [4]. The requirements posed by quantum computers on the control circuitry translate to extremely demanding specifications in terms of the noise and power budget, calling for careful system design and optimization [5]. To meet the specifications of the system and to analyze the impact of non-idealities in both the classical and the quantum sub-systems, a tightly coupled co-simulation of the classical controller with the quantum system is of fundamental importance. Moreover, performing such a co-simulation in a common design environment will enable the design and automation of small-scale quantum processors, which is lacking in the current state of the art.

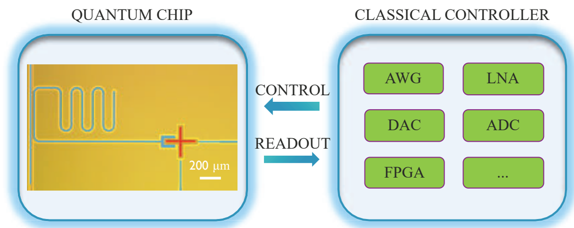

Fig. 1. Schematic representation of the core of a quantum computer, consisting of a quantum chip and a classical controller.

The dynamics of quantum systems are normally described using differential equations. Since SPICE (Simulation Program with Integrated Circuit Emphasis) based circuit simulators are well-adapted to solving differential equations [6], they can also be used to simulate quantum systems, provided that an accurate equivalent circuit is generated for them, which comprehensively describes the relevant quantum behavior. An equivalent circuit representation for Coulomb-coupled and metal-contacted nanoscale quantum devices has previously been proposed [7], where the dynamics of the system are described using quantum Markovian master equations. This method was used to derive linear circuit models for describing the interaction between a superconducting qubit and a resonator [8], [9]. However, these works included major approximations, where the resonator was treated as a classical entity [8], and the quantum mechanical correlations between the qubit and the resonator photons were ignored [9]. A co-design and co-optimization strategy for quantum-classical systems was also proposed in [10], where a Verilog-A model based on the Hamiltonian of the quantum system was used to simulate the time evolution of the system. However, this approach is limited to quantum systems that do not interact with their environment, and does not consider the imperfections, such as energy relaxation and decoherence. Hence, they cannot deal with the entire range of non-idealities that are critical to accurately model the system. Moreover, the readout of the qubit state, taking the control electronics into account, was not implemented in prior works either.

In this paper, we develop a systematic methodology to transform the description of a quantum mechanical system, including its non-idealities, to equivalent circuits. Specifically, we use this approach to develop a model that completely describes a quantum system that consists of a superconducting qubit coupled to a superconducting resonator. The model is used in the Cadence® Spectre® circuit simulator to simulate the control and readout of the qubit, while considering non-ideal effects such as qubit energy relaxation and decoherence. We further include higher energy states of the qubit that are always present but usually neglected for simplicity (i.e., beyond the qubit or 2-level approximation), which impacts the control of the qubit. To the best of our knowledge, this is the first demonstration of the control and readout of the qubit performed completely in an electrical circuit simulation environment, taking into account the non-idealities in the system. Therefore, the incorporation of the readout and the modelling of the non-idealities are the main contributions of the paper.

The paper is organized as follows: Section II will introduce the systematic methodology used to convert the description of a quantum system to an equivalent circuit. In Section III, the simulation results demonstrating the unique features of our approach, namely the readout, control, and measurement of qubit relaxation and decoherence will be shown. Final conclusions will be drawn in Section IV.

II. Methodology

A. Description of a quantum system with circuit models

In quantum mechanics, the state $|\Psi\rangle$ of a quantum system is described as a vector in an n-dimensional complex vector space, known as the Hilbert space. The unitary time evolution of the state is governed by the Hamiltonian H of the system (see Section III for examples), which is an $n \times n$-dimensional matrix that represents the total energy of the system. The state vectors that lie on a unit sphere in the vector space are called pure states. Note that an arbitrary superposition of pure states is also a pure state. However, the state of the system can also be a statistical mixture of different pure states, in which case it is known as a mixed state. In this scenario, the system is best described by an $n \times n$-dimensional matrix called the density matrix:

$$\rho = \sum_i p_i \left|\Psi_i\right\rangle \left\langle\Psi_i\right|, \tag{1}$$

where p_i is the probability of being in the pure state $|\Psi_i\rangle$. The unitary time-evolution of the system is described by the Liouville-von Neumann equation:

$$\dot{\rho}(t) = -\frac{i}{\hbar}\big(H\rho(t) - \rho(t)H\big), \tag{2}$$

where $\hbar$ is the reduced Planck constant, and i is the unit imaginary number. Equation (2) is a compact representation of a family of coupled differential equations, and can readily be solved using numerical solvers. In order to illustrate this further, consider a 2-level system (such as a qubit), which is described using a Hamiltonian H and a density matrix ρ, with $H, \rho \in \mathcal{M}_{2\times 2}(\mathbb{C})$

$$\begin{aligned} \rho &= \begin{bmatrix} \rho_{00} & \rho_{01} \\ \rho_{10} & \rho_{11} \end{bmatrix} \\ H &= \begin{bmatrix} H_{00} & H_{01} \\ H_{10} & H_{11} \end{bmatrix} \end{aligned} \tag{3}$$

Combing (2) and (3), we infer the following:

$$\begin{aligned} i\hbar\dot{\rho}_{00}(t) &= + H_{01}\rho_{10}(t) - H_{10}\rho_{01}(t) \\ i\hbar\dot{\rho}_{01}(t) &= + H_{00}\rho_{01}(t) - H_{01}\rho_{00}(t) \\ &\quad + H_{01}\rho_{11}(t) - H_{11}\rho_{01}(t) \\ i\hbar\dot{\rho}_{10}(t) &= - H_{00}\rho_{10}(t) + H_{10}\rho_{00}(t) \\ &\quad - H_{10}\rho_{11}(t) + H_{11}\rho_{10}(t) \\ i\hbar\dot{\rho}_{11}(t) &= - H_{01}\rho_{10}(t) + H_{10}\rho_{01}(t) \end{aligned} \tag{4}$$

Each of these individual equations uses complex values and can be converted to two real-valued equations by separating the real and imaginary parts, resulting in $8 (= 2n^2)$ equations. Using the properties of density matrices (unit trace and hermicity i.e., $\rho_{ij} = \rho^*_{ji}$), these can be reduced to $3 (= n^2 - 1)$ real-valued equations for the 2-dimensional system, each having the functional form:

$$\dot{\lambda}_i(t) = \sum_{j=1}^{n^2-1} G_{ij}\lambda_j(t), \tag{5}$$

where λ_i are real-valued functions, and G_{ij} are coefficients determined by H. Interestingly, (5) has the form of Kirchhoff's current law (KCL) at a node with a capacitor being charged by a set of voltage-dependent current sources, and thus can be easily solved in a SPICE-type circuit simulator. For this, each λ_i is represented as the voltage across a capacitor C_i connected to a node i in the circuit, with behavioral current sources charging the node i with currents $C_i G_{ij} \lambda_j$ (see Fig. 2). The solution to KCL at all the nodes provides the solution to the time evolution of the density matrix of the quantum system. The quantum system governed by (2) is a closed system exhibiting aforementioned unitary dynamics. However, in practice, a quantum system will always interact with its environment, resulting in losses in the form of energy relaxation and decoherence [11]. In addition to this uncontrolled part of the environment, the system also needs to be coupled with the external world for measurement and control. In both cases, the internal dynamics of the system due to these environmental interactions can be described using quantum master equations. We use the master equation in the Lindblad form [12], which defines the time evolution of the density matrix ρ as:

$$\begin{aligned} \dot{\rho}(t) = &- \frac{i}{\hbar}\big(H_T\rho(t) - \rho(t)H_T\big) \\ &+ \frac{1}{2}\sum_i \kappa_i\big(2L_i\rho(t)L_i^\dagger - L_i^\dagger L_i\rho(t) - \rho(t)L_i^\dagger L_i\big) \end{aligned} \tag{6}$$

where $H_T = H + H_D$, H_D is the Hamiltonian corresponding to the external drive, and L_i are known as the Lindblad or jump operators, while κ_i are the corresponding coupling rates to the

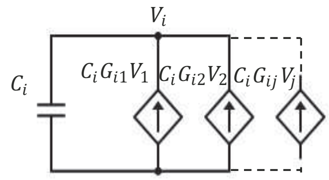

Fig. 2. Equivalent circuit at a node for solving (5) where a capacitor C_i connected to node i is charged by a set of voltage-controlled current sources, such that the voltage across the capacitor $V_i = \lambda_i$.

environment. The Lindblad operators capture the correlations of the system with the uncontrolled degrees of freedom in the environment, resulting in the mixed states. Even though (6) seems more complex than (2), the solution of the differential equation will still take the functional form of (5), and can thus be implemented using equivalent circuits based on capacitors and behavioral current sources. We therefore emphasize that the resultant model still remains fully compatible with SPICE-type circuit simulators.

B. Co-simulation of quantum system with control electronics

The method employed for the co-simulation of the quantum system with the control electronics is described in Fig. 3. First, the parameters of the quantum system (see Table 1 for examples) required for defining the Hamiltonian and the Lindblad operators are represented in symbolic notation. We use Python-based packages QuTiP [13] and Sympy [14] to achieve this, although other programming languages can also be used. Symbolic matrix expansion based on (6) is performed in Python and processed further to take it to the form shown in (5). Once this is performed, the netlist of the equivalent circuit can efficiently be generated, node by node. The symbolic parameters of the system are also transformed into parameters in the netlist, thereby allowing to run parametric simulations without having to regenerate the circuit. Once the netlist is generated, it is interfaced with the additional electronic control circuits required for the manipulation of the quantum system. Using 4 threads in Cadence® Spectre®, the typical timescale for the simulation of a simple quantum system is of the order

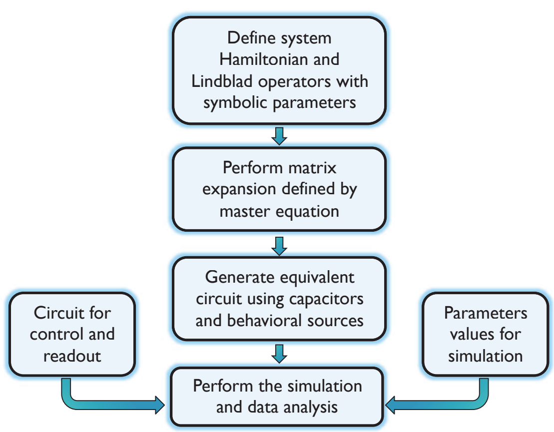

Fig. 3. Method for the co-simulation of a quantum system with classical control electronics.

of a few minutes with a peak memory usage of ∼150 MB. Since we aim to represent the complete quantum mechanical behavior, without a priori simplifications, the complexity grows exponentially with the number of qubits, due to the underlying principles of quantum mechanics. While simplifications are certainly possible in particular situations, at present we advocate this methodology to be used for the co-simulation of small-scale quantum systems, which form the building block for larger systems.

III. Results : Simulation of qubit operation with non-idealities

In this section, we will use the presented methodology to simulate the fundamental superconducting quantum system, a resonator coupled to a qubit. The simulations are focused on the behavior of the quantum system, and the required classical control signals are currently modelled using ideal behavioral sources. Unless specified otherwise, the parameter values used in the simulations are as listed in Table I.

A. Qubit readout

In superconducting quantum circuits, the readout of the qubit state is achieved by coupling it to a superconducting resonator. The Hamiltonian describing this interaction [15] is given by:

$$H_1 = \hbar\omega_r a^\dagger a + \hbar\omega_q \sigma_z/2 + \hbar g(a^\dagger\sigma^- + a\sigma^+), \qquad (7)$$

where $\omega_r(\omega_q)$ is the frequency of the resonator (qubit), g is the coupling strength between the qubit and the resonator, $a^\dagger(a)$ is the photon creation (annihilation) operator, $\sigma^+(\sigma^-)$ is the qubit raising (lowering) operator, and σ_z is the Pauli-Z operator. The Lindblad operator corresponding to the finite linewidth of the resonator is given below:

$$L_1 = \frac{\kappa}{2}\big(2a\rho a^\dagger - a^\dagger a\rho - \rho a^\dagger a\big), \qquad (8)$$

where κ is the decay rate of the resonator, such that the quality factor $Q = \omega_r/\kappa$. The qubit-resonator system is normally operated with a detuning $\Delta(= \omega_q - \omega_r)$ between the qubit frequency and the resonator frequency, such that the ratio $|g/\Delta| \ll 1$ – the so-called dispersive coupling regime. In this limit, the resonator and the qubit can, to first order, be described as operating independently. The coupling between them results in a shift in the frequency response of the resonator that depends on the state of the qubit (refer Fig. 4(a)), allowing to gain information about the qubit by probing the resonator.

In a standard experiment, the readout of the qubit is performed by applying a microwave pulse to the resonator at a frequency ω_{LO}. The signal interacts with the resonator,

TABLE I
Typical values used for the system parameters in the simulations

Parameter	Symbol	Value
Qubit frequency	$\omega_q/2\pi$	4 GHz
Resonator frequency	$\omega_r/2\pi$	5 GHz
Qubit-resonator coupling	$g/2\pi$	50 MHz
Resonator decay rate	$\kappa/2\pi$	10 MHz

populating it with microwave photons, and produces an output signal with an amplitude that is directly proportional to the electric field in the resonator. The output voltage $s(t)$ can be obtained using the input-output theory [16] and has the form:

$$s(t) = A\cos(\omega_{LO}t + \theta), \tag{9}$$

where A and θ represent the amplitude and phase response, respectively. If $\omega_{LO} = \omega_r$, the information about the qubit state is encoded in the phase θ, which can be extracted by a homodyne demodulation scheme, as shown in Fig. 4(b). The

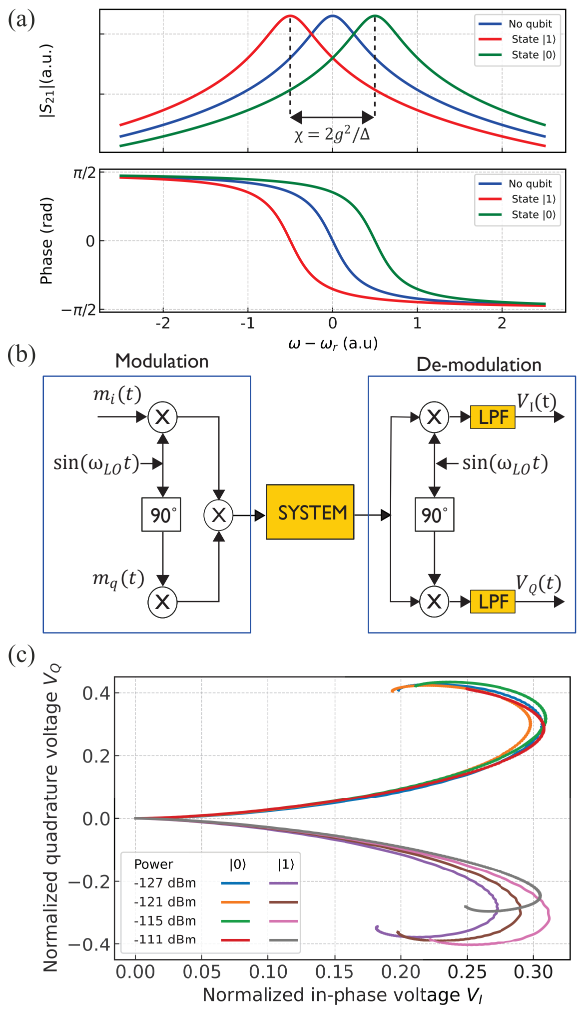

Fig. 4. (a) Amplitude (top panel) and phase (bottom panel) response of a resonator measured in transmission mode, in the absence of coupling to the qubit (blue), and with dispersive coupling to the qubit when the qubit is in state $|0\rangle$ (green) or state $|1\rangle$ (red). The dispersive shift in the presence of the qubit is given by $\chi = (2g^2)/\Delta$. (b) A generic scheme for I-Q modulation and demodulation. The carrier is modulated by an in-phase signal $m_i(t)$ and the carrier quadrature is modulated by $m_q(t)$. The demodulation results in the in-phase voltage (V_I) and the quadrature voltage (V_Q) at the output of the low-pass filters (LPF). For the readout pulse, we do not use the Q channel in the modulator. (c) Normalized (to the microwave power) plot of V_q versus V_I measured for the qubit initialized in the states $|0\rangle$ and $|1\rangle$. The measured phase angle $\tan^{-1}(V_Q/V_I)$ has opposite signs for the two states, allowing state detection. With an increase in microwave power, there is a change in the measured phase due to the excitation of the qubit by the resonator photons.

measured readout signal, in terms of the in-phase (V_I) and the quadrature (V_Q) voltages, can be used to extract the phase angle as $\tan^{-1}(V_Q/V_I)$. Fig. 4(c) shows the results obtained by measuring V_I and V_Q for various microwave powers when the qubit is initialized in states $|0\rangle$ and $|1\rangle$. It is clearly seen that the curves corresponding to the two states move in opposite directions, thus enabling the readout of the qubit state by measuring the phase of the readout signal. We also notice that with an increase in microwave power, there is a change in the measured phase angle between the two states. At higher powers, a larger number of photons is present in the resonator, causing an effective excitation on the qubit. For readout, we also emphasize that the resonator drive should be chosen such that this number does not exceed the critical photon number $n_{crit} = \Delta^2/(4g^2)$ [15], [17]. Note that the readout of the qubit using demodulation has not been considered in prior works.

B. Qubit Control

For the realization of quantum algorithms, it is also essential to control the state of the qubit. This is achieved by applying a microwave control pulse to the qubit. The coupling of the qubit to the drive can be described by the following Hamiltonian [17]:

$$H_{qd} = i\Omega_d V_d(t)(\sigma^- - \sigma^+), \tag{10}$$

where $V_d(t) = V_0 f(t)\cos(\omega_d t + \phi)$ is the microwave drive with an amplitude V_0, pulse shape $f(t)$, frequency ω_d and phase ϕ. Ω_d is a measure of the coupling strength of the drive to the charge degree of freedom of the qubit. Starting from state $|0\rangle$, the qubit can be driven to an arbitrary state $c_1|0\rangle + c_2|1\rangle$ by choosing an appropriate pulse shape, frequency, phase, amplitude and duration.

The most commonly used superconducting qubits, like the transmon [18] and the xmon [19], are not pure 2-level systems, but consist of several higher-energy states. Particularly, the presence of the higher-energy state $|2\rangle$ is taken into account using a design parameter called the qubit anharmonicity α , and is defined as $\alpha = \omega_{21} - \omega_{10}$. Here $\hbar\omega_{ij}$ is the energy separation between the states $|i\rangle$ and $|j\rangle$. Superconducting qubits have relatively low anharmonicity ($\alpha/2\pi \simeq$ 200-400 MHz, which imposes restrictions on the shape and bandwidth of the control signal. The pulse must be carefully chosen to prevent the leakage of excitations from the computational states of $|0\rangle$ and $|1\rangle$ to higher-order states. For this purpose, it is essential to include higher states in the model, since such non-idealities notably affect real-world quantum-classical systems and are thus imperative for system design and optimization. To perform a qubit operation and verify its functionality, a control pulse is first applied to the qubit followed by the readout of the qubit state using a readout pulse, as sketched in Fig. 5(a). Restricting the qubit to a 2-level system with states $|0\rangle$ and $|1\rangle$, a simple square pulse results in an oscillation, known as Rabi oscillation, between the two states (blue curve in Fig. 5(b)). However, with the inclusion of the third state $|2\rangle$, the measured phase of the readout signal is significantly distorted when using a square pulse for excitation (orange curve in Fig. 5(b)). This is because short square pulses, when analyzed in the frequency domain, have large frequency bandwidth and therefore finite power at the frequency of the $|1\rangle \rightarrow |2\rangle$ transition. Such pulses can thus result in excitation leakage from the computational states to state $|2\rangle$. The larger negative phase in the measured readout signal is also attributed to this leakage. This issue is well known and can be avoided by pulse engineering techniques, for example using DRAG pulses [20], [21]. In this scheme, a Gaussian pulse and its derivate are applied to the carrier signal and its quadrature, respectively, to produce an I-Q-modulated control signal (refer to the modulation block in Fig. 4(b)). As shown in Fig. 5(b), excitation of the qubit with the DRAG pulse (green curve) shows a smooth oscillatory behavior, similar to the Rabi oscillations of the 2-level qubit system. Since our framework can involve many such non-idealities, we can accurately model the effects of pulse engineering. It is interesting to note that even with DRAG pulse, at short pulse durations, we observe a leakage to the state $|2\rangle$, allowing us to investigate the limits of such first-order compensation schemes. Obviously, these effects are much lower in comparison to the case with the square pulse, in line with them now being higher order effects; nevertheless, they allow us to identify limits on the achievable control fidelity.

C. Relaxation and decoherence

With the ability to perform qubit control and readout, we can now simulate the experiments used to measure the relaxation and decoherence times of the qubit.

1) Energy relaxation: Relaxation is the process through which the energy in the qubit is lost due to its interaction with the environment. This can be included in the qubit dynamics using the following Lindblad operator:

$$L_2 = \frac{\gamma_1}{2}\left(2\sigma^-\rho\sigma^+ - \sigma^+\sigma^-\rho - \rho\sigma^+\sigma^-\right), \tag{11}$$

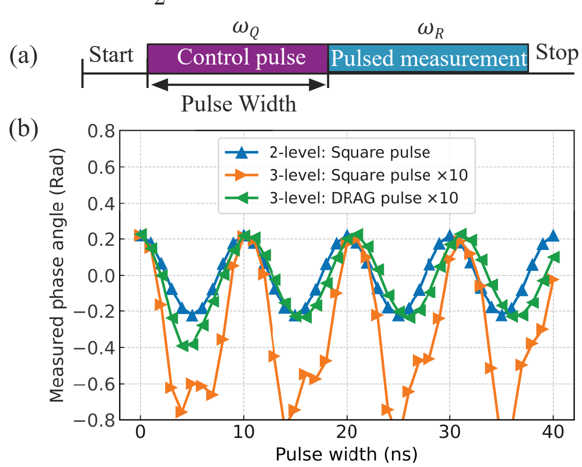

Fig. 5. (a) Pulse sequence for control and readout of the qubit state. (b) Measured phase angle as a function of the pulse duration, exhibiting Rabi oscillations. For a 2-level system, an excitation with a square pulse results in a smooth oscillatory behavior (blue). With the inclusion of the higher-order $|2\rangle$ state with an anharmonicity $\alpha = 2\pi \times 200\,\text{MHz}$, the square pulse causes significant distortion due to leakage (orange). Smooth oscillatory behavior is observed when using DRAG pulses for qubit excitation (green). The simulation was performed with $\Omega_d = 2\pi \times 1\,\text{THz/V}$ and a pulse amplitude of $100\,\mu\text{V}$, resulting in a Rabi frequency of 100 MHz. For the DRAG pulses, we defined the pulse duration as 4σ, where σ is the standard deviation of the underlying Gaussian function.

where $\gamma_1 = 1/T_1$ is the energy relaxation rate with the relaxation time T_1. The measurement of the relaxation time begins with an application of a π-pulse that prepares the qubit in the excited state, followed by the readout of the qubit state, after waiting for a certain delay time in which the qubit can decay (refer Fig. 6(a)).

In addition to the intrinsic relaxation rate, the qubit energy also decays via the resonator, known as the Purcell decay [17], with the decay rate given by $\gamma_P = 1/T_P = \kappa g^2/\Delta^2$. The measured relaxation rate in an experiment is a combination of these two rates such that $1/T_{1(\text{measured})} = 1/T_1 + 1/T_P$.

Fig. 6(b) shows the measured phase angle and the corresponding qubit population (inset) as a function of the pulse delay for different detunings Δ. As Δ becomes smaller, the Purcell decay becomes larger, but the dispersive shift $((2g^2)/\Delta)$ is also larger, resulting in a larger readout signal, and vice versa. This shows that the choice of design parameters can have a significant impact on the behavior of the underlying quantum system and its measurement using control circuity, which is captured accurately in our simulations.

2) Decoherence: A superposition state $c_0|0\rangle + c_1|1\rangle$ has a well-defined phase between the two basis states. Decoherence is the process through which the qubit loses this phase information. It can be included in the qubit dynamics using the operator:

$$L_3 = \frac{\gamma_\phi}{2}\frac{1}{2}\left(2\sigma_z\rho\sigma_z - \sigma_z\sigma_z\rho - \rho\sigma_z\sigma_z\right), \tag{12}$$

where $\gamma_\phi = 1/T_\phi$ is known as the pure dephasing rate and T_ϕ is the pure dephasing time. The measurement of the decoherence can be performed using a Ramsey experiment where two $\pi/2$-pulses are applied to the qubit, separated by a delay time during which the qubit can evolve freely. This is followed

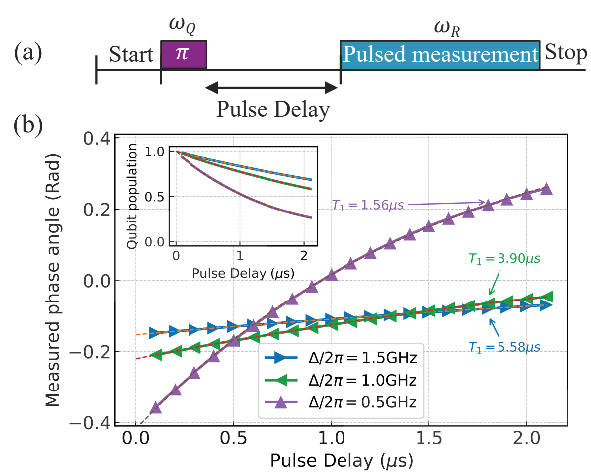

Fig. 6. (a) Pulse sequence for measurement of the qubit relaxation time. (b) Measured phase angle and extracted qubit population (inset) as a function of the pulse delay for different detunings Δ. The relaxation time is extracted based on an exponential fit to the measured phase angle. The simulation was performed with an intrinsic relaxation time $T_1 = 10\mu\text{s}$. We note that the measured relaxation time is always smaller than the intrinsic value due to the additional Purcell decay time $T_P = \Delta^2/(g^2\kappa)$, such that $1/T_{1(\text{measured})} = 1/T_1 + 1/T_P$. $T_P = 14.32\,\mu\text{s}, 6.36\,\mu\text{s}$ and $1.59\,\mu\text{s}$ for $\Delta = 1.5\,\text{GHz}, 1.0\,\text{GHz}$ and $0.5\,\text{GHz}$, respectively.

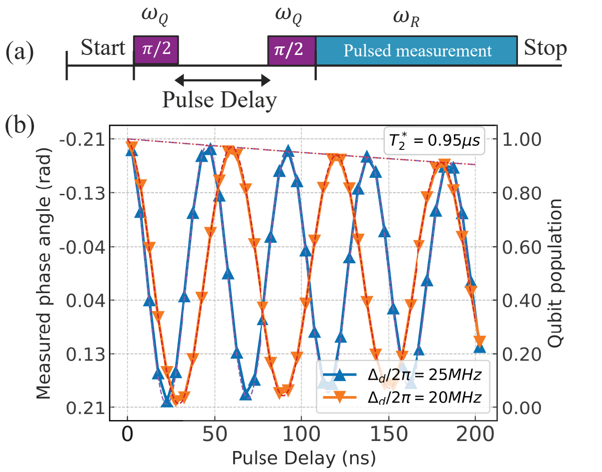

Fig. 7. (a) Pulse sequence for the measurement of qubit decoherence time by a Ramsey experiment. (b) Measured phase angle (left y-axis) and extracted qubit population (right y-axis) as a function of the pulse delay time for different drive detunings Δ_d. The T_2^* time is extracted using an exponentially decaying cosine to the measured phase angle. The simulation was performed with a dephasing time $T_\phi = 1\,\mu s$ and $T_1 = 10\,\mu s$. It can be seen that the measured T_2^* is close to the T_ϕ time as the contributions from the qubit relaxation are significantly low for the given choice of parameters. With an increase in Δ_d, the oscillation frequency also shifts to a larger frequency.

by a readout pulse to measure the qubit state (refer Fig. 7(a)). As shown in Fig. 7(b), for a given detuning $\Delta_d = \omega_d - \omega_q$ of the microwave drive to the qubit frequency, the measured phase angle exhibits decaying oscillations. In a Ramsey experiment, the measured decoherence time T_2^* is a combination of the pure dephasing time as well as decoherence caused due to the energy relaxation, and is given by $1/T_2^* = 1/2T_1 + 1/T_\phi$. Its dependence on different system-level parameters in the experiment can accurately be simulated with our methodology.

IV. Conclusion

A systematic methodology has been proposed to transform the behavior of small-scale quantum systems to equivalent circuit models that can be used in a generic electrical simulator in tight combination with models for conventional circuits for readout and control. The approach has been validated by simulating the control and readout of a superconducting qubit-resonator quantum system. The circuit-level simulations mimic realistic experiments and allow to incorporate and analyze the impact of important non-idealities such as qubit relaxation, decoherence and leakage to non-computational states, which is unique for our approach. The simulation results show excellent agreement with analytical theory of the quantum devices. This validates that the proposed methodology is extremely useful for the co-simulation of small-scale qubit devices with their control circuitry. Future works will employ this methodology to determine the design specifications of the control electronics required for optimal qubit operations, which can then be leveraged for larger-scale quantum systems.

Acknowledgment

This work was supported in part by the imec Industrial Affiliation Program on Quantum Computing.

References

[1] J. Preskill, "Quantum computing in the NISQ era and beyond," *Quantum*, vol. 2, p. 79, Aug. 6, 2018. arXiv: 1801.00862.

[2] F. Arute *et al.*, "Quantum supremacy using a programmable superconducting processor," *Nature*, vol. 574, no. 7779, pp. 505–510, Oct. 2019.

[3] M. Mehrpoo *et al.*, "Benefits and challenges of designing cryogenic CMOS RF circuits for quantum computers," in *2019 IEEE International Symposium on Circuits and Systems (ISCAS)*, Sapporo, Japan: IEEE, May 2019, pp. 1–5.

[4] J. C. Bardin *et al.*, "Design and characterization of a 28-nm bulk-CMOS cryogenic quantum controller dissipating less than 2 mW at 3 k," *IEEE Journal of Solid-State Circuits*, vol. 54, no. 11, pp. 3043–3060, Nov. 2019.

[5] F. Sebastiano *et al.*, "Cryo-CMOS electronic control for scalable quantum computing: Invited," in *Proceedings of the 54th Annual Design Automation Conference 2017*, Austin TX USA: ACM, Jun. 18, 2017, pp. 1–6.

[6] W. Zimmerman, "Time domain solutions to partial differential equations using SPICE," *IEEE Transactions on Education*, vol. 39, no. 4, pp. 563–573, Nov. 1996.

[7] Á. Csurgay and W. Porod, "Equivalent circuit representation of arrays composed of coulomb-coupled nanoscale devices: Modelling, simulation and realizability," *International Journal of Circuit Theory and Applications*, vol. 29, no. 1, pp. 3–35, 2001.

[8] G. Csaba, Z. Fahem, F. Peretti, and P. Lugli, "Circuit modeling of flux qubits interacting with superconducting waveguides," *Journal of Computational Electronics*, vol. 6, no. 1, pp. 105–108, Apr. 9, 2007.

[9] A. Matyas, C. Jirauschek, F. Peretti, P. Lugli, and G. Csaba, "Linear circuit models for on-chip quantum electrodynamics," *IEEE Transactions on Microwave Theory and Techniques*, vol. 59, no. 1, pp. 65–71, Jan. 2011.

[10] J. v. Dijk, A. Vladimirescu, M. Babaie, E. Charbon, and F. Sebastiano, "SPINE (SPIN emulator) - a quantum-electronics interface simulator," in *2019 IEEE 8th International Workshop on Advances in Sensors and Interfaces (IWASI)*, Otranto, Italy: IEEE, Jun. 2019, pp. 23–28.

[11] M. A. Nielsen and I. L. Chuang, *Quantum computation and quantum information*, 10th anniversary ed. Cambridge ; New York: Cambridge University Press, 2010, 676 pp.

[12] D. Manzano, "A short introduction to the lindblad master equation," *AIP Advances*, vol. 10, no. 2, p. 025 106, Feb. 1, 2020. arXiv: 1906.04478.

[13] J. Johansson, P. Nation, and F. Nori, "QuTiP 2: A python framework for the dynamics of open quantum systems," *Computer Physics Communications*, vol. 184, no. 4, pp. 1234–1240, Apr. 2013.

[14] A. Meurer *et al.*, "SymPy: Symbolic computing in python," *PeerJ Computer Science*, vol. 3, e103, Jan. 2, 2017.

[15] A. Blais, R.-S. Huang, A. Wallraff, S. M. Girvin, and R. J. Schoelkopf, "Cavity quantum electrodynamics for superconducting electrical circuits: An architecture for quantum computation," *Physical Review A*, vol. 69, no. 6, p. 062 320, Jun. 29, 2004.

[16] A. A. Clerk, M. H. Devoret, S. M. Girvin, F. Marquardt, and R. J. Schoelkopf, "Introduction to quantum noise, measurement, and amplification," *Reviews of Modern Physics*, vol. 82, no. 2, pp. 1155–1208, Apr. 15, 2010.

[17] P. Krantz, M. Kjaergaard, F. Yan, T. P. Orlando, S. Gustavsson, and W. D. Oliver, "A quantum engineer's guide to superconducting qubits," *Applied Physics Reviews*, vol. 6, no. 2, p. 021 318, Jun. 2019.

[18] J. Koch *et al.*, "Charge-insensitive qubit design derived from the cooper pair box," *Physical Review A*, vol. 76, no. 4, p. 042 319, Oct. 12, 2007.

[19] R. Barends *et al.*, "Coherent josephson qubit suitable for scalable quantum integrated circuits," *Physical Review Letters*, vol. 111, no. 8, p. 080 502, Aug. 22, 2013.

[20] F. Motzoi, J. M. Gambetta, P. Rebentrost, and F. K. Wilhelm, "Simple pulses for elimination of leakage in weakly nonlinear qubits," *Physical Review Letters*, vol. 103, no. 11, p. 110 501, Sep. 8, 2009.

[21] J. M. Gambetta, F. Motzoi, S. T. Merkel, and F. K. Wilhelm, "Analytic control methods for high-fidelity unitary operations in a weakly nonlinear oscillator," *Physical Review A*, vol. 83, no. 1, p. 012 308, Jan. 18, 2011.